Received: 4 August 2024 | *Revised:* 3 September 2024 | *Accepted:* 17 September 2024
DOI: 10.37917/ijeee.20.2.25 *Vol. 20 | Issue 2 | December 2024*

Iraqi Journal for Electrical and Electronic Engineering
Original Article

Open Access
IJEEE University of Basrah College of Engineering

Lyapunov Function Control Strategy for a Three-Phase Grid-Tied LCL Filtered Quasi Z-Source Inverter (qZSI)

Ali Kadhim Abdulabbas*, Shafaa Mahdi Salih
Electrical Engineering Department, University of Basrah, Basra, Iraq

Correspondance
*Ali Kadhim Abdulabbas
Electrical Engineering Department
University of Basrah, Basra, Iraq
Email: ali.abdulabbas@uobasrah.edu.iq

Abstract
The presented research introduces a control strategy for a three-phase grid-tied LCL-filtered quasi-Z-source inverter (qZSI) using a Lyapunov-function-based method and cascaded proportional-resonant (PR) controllers. The suggested control strategy ensures the overall stability of the closed-loop system and eliminates any steady-state inaccuracy in the grid current. The inverter current and capacitor voltage reference values of qZSI are created by the utilization of cascaded coupled proportional-resonant (PR) controllers. By utilizing synchronous reference frame and Lyapunov function- based control, the requirement to perform derivative operations and anticipate inductance and capacitance are avoided, resulting in achieving the goal of zero steady-state error in the grid current. The qZSI can accomplish shoot-through control by utilizing a simple boost control method. Computer simulations demonstrate that the suggested control strategy effectively achieves the desired control objectives, both in terms of steady-state and dynamic performance.

Keywords
Grid Tied LCL Filter, Lyapunov Function-based Control, Shoot-through Modulation, Proportional Resonant Control, Quasi Z-source Inverter.

I. Introduction

The increasing popularity of Renewable Energy Sources (RESs) and their integration into the power grid received significant attention in recent years [1]. In general, the transmission of electricity from an RES to the electrical grid is made possible by voltage source inverters (VSIs) that operate using advanced control methods to meet the specified regulations and standards. Nevertheless, it is widely acknowledged that the output voltage derived from an RES is not consistently stable. Consequently, if the RES operates below the designated threshold level, the VSI becomes unable to operate effectively. Although Current Source Inverters (CSIs) can increase their input voltage, they are rarely favored in these applications due to the complexity of control algorithms [2]. Another choice is to establish a connection between the RES and VSI by utilizing a dc/dc boost converter. However, the inclusion of an additional power stage necessitates an increase in the number of switches, resulting in higher costs and reduced efficiency and system reliability [3, 4].

To overcome these limitations, alternate converter topologies, such as the Z-source inverter (ZSI) and quasi-Z-source inverter (qZSI), have been established [5, 6]. These inverter topologies incorporate an impedance network positioned between the Direct Current (DC) supply and the inverter. The primary purpose of joining the impedance network is to enable the implementation of shoot-through states, where in the switching devices on the same inverter leg are simultaneously triggered. This can allow the DC input voltage to be amplified to the required level using the impedance network. Both topologies possess the capability to boost or buck DC input voltage [7]. The qZSI has gained increased attention because of its capability to deliver uninterrupted input current and minimize component stress in the impedance network [8–18]. The performance of qZSI-based systems is dependent upon

the technique employed to regulate the inverter. Typically, the control process consists of two main objectives: producing active states and generating shoot-through states. While the first task is accomplished by typical control methods, the latter can be readily achieved using the simple boost control technique outlined in [9].

The qZSI investigations focus on single-phase grid-linked systems [10–12], uninterruptible power supply systems [13–15], three-phase grid-tied systems [16], [17], and three-phase four-leg uninterruptible power supply systems [18]. A control approach is proposed in [10] for effectively managing a grid-tied cascaded multilevel qZSI solar power plant. The proposed control method, as described in [11], effectively reduces the necessary capacitance value in the impedance network by implementing improved modulation and double-frequency ripple suppression techniques. In [12], a hybrid pulsewidth modulation (HPWM) technique is suggested, which mixes the pulsewidth modulation and pulse-amplitude modulation schemes. The current ripple damping control is introduced in [13]. The control methods described in references [12]and [13] result in a decrease in the required inductance and capacitance values in the impedance network. However, in all of the aforementioned approaches suggested for single- and three-phase grid-tied systems, the Voltage Source Inverter (VSI) is connected to the grid using an L filter instead of an LCL filter.

This work investigates the suitability of using a Lyapunov-function-based control technique to regulate a three-phase grid-tied qZSI with an LCL filter. The LCL filter is widely recognized for introducing two extra poles into the system, which poses challenges in designing the control technique due to the potential for instability and the need for resonant damping. Ensuring global stability for such a system is crucial because of the inherent stability difficulty with the LCL filter. A recent study [19] has demonstrated that the control approach based on Lyapunov functions ensures global stability of the three-phase grid-tied LCL-filtered VSI, even when subjected to significant perturbations deviating from the operational point. The inverter current and capacitor voltage reference are determined by a proportional-resonant (PR) control mechanism. In contrast to the work described in reference [19], this study proposes a method to establish inverter current and capacitor voltage references of three-phase inverter by employing basic equations derived from synchronous reference frame. The capacitor voltage and inductor current reference of qZSI are produced by a two proportional-resonant (PR) controller that is linked to the output of the primary controller manipulating the inductor current error, with the inverter current reference being generated by the initial proportional-resonant (PR) controller. Theoretical considerations are validated using computer simulations.

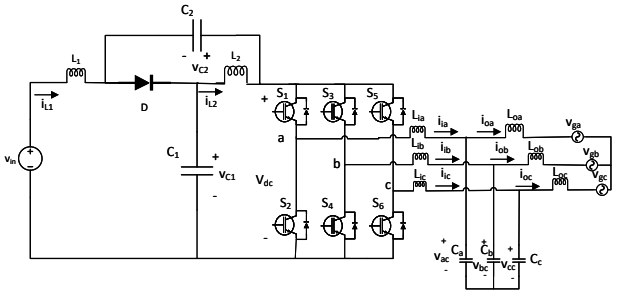

Fig. 1. The overall configuration of a three-phase quasi-Z-source inverter (qZSI) connected to a grid with an LCL filter.

II. Mathematical Depiction of The System

Fig. 1 depicts a three-phase grid-tied LCL-filtered quasi-Z-source inverter (qZSI). The mathematical representations of the quasi-source network and voltage source inverter are provided in the subsequent sections.

1) Quasi-Z-Source Inverter Circuit modeling

Similar to the conventional ZSI, the qZSI also has two operational states on the DC side: the active state (which includes the six active states and two conventional zero states of the traditional VSI) and the shoot-through state (where both switches in at least one phase conduct simultaneously). When observed from the DC side, the inverter bridge behaves like a current source in cases of the active state. Two states can be represented by their respective equivalent circuits, which are illustrated in Fig. 2. The shoot-through state is not allowed in the conventional Voltage Source Inverter (VSI) due to the risk of short-circuiting the voltage source, which might result in device damage. The qZSI and ZSI, when combined with the LC and diode network, alter the functioning of the circuit, enabling the shoot-through state.

For general analysis, the input voltage, v_{in}, is selected as the system input, which is related to the input current, i_{L1}. The reason for this is that RES does not possess the same rigid output characteristics as an ideal voltage source or current source. In DC-side modeling, the three-phase inverter bridge and external AC load are simplified as a single switch and current source connected in parallel [20]. The asymmetric quasi-Z-source network has four state variables: The currents flowing through the inductors are denoted as i_{L1} and i_{L2}, The voltage over the capacitors v_{C1} and v_{C2}. The independent load current, i_{load}, operates as an additional input or disturbance to the quasi-Z-source network. Select v_{C1} and i (also known

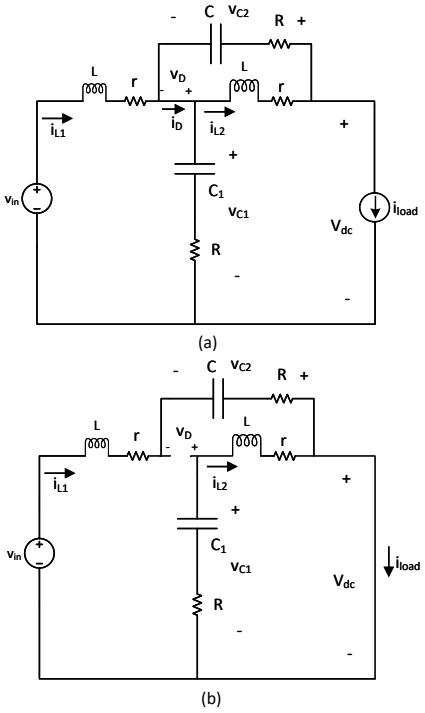

Fig. 2. The equivalent circuit of the quasi-Z-source inverter (qZSI) can be represented in two states: (a) the active state and (b) the shoot-through state.

as i_{in}) as the output variables for the analyzed system. In order simplification, assume that $C = C_1 = C_2$, $L = L_1 = L_2$, the stray resistances of inductors $r = r_1 = r_2$, the Equivalent Series Resistances (ESR) of capacitors $R = R_1 = R_2$. The shoot-through interval T_0 refers to the duration during which both switches are turned on simultaneously. The active interval T_1, on the other hand, is the duration when only one switch is turned on in one leg. The switching period T is the sum of T_0 and T_1. The shoot-through duty ratio, denoted as D_0, is calculated by dividing T_0 by T. The state space model of the qZSI in the two intervals (active and shoot-through) can be given in Eq. (1).

$$\begin{aligned} \frac{d\mathbf{x}}{dt} &= \mathbf{A}\mathbf{x} + \mathbf{B}\mathbf{u} \\ \mathbf{y} &= \mathbf{C}\mathbf{x} + \mathbf{D}\mathbf{u} \end{aligned} \tag{1}$$

where

$$\mathbf{A} = \begin{bmatrix} -\frac{(r+R)}{L} & 0 & -\frac{1}{L}(1-d_o) & \frac{1}{L}d_o \\ 0 & -\frac{(r+R)}{L} & \frac{1}{L}d_o & -\frac{1}{L}(1-d_o) \\ \frac{1}{L}(1-d_o) & -\frac{1}{C}d_o & 0 & 0 \\ -\frac{1}{C}d_o & \frac{1}{C}(1-d_o) & 0 & 0 \end{bmatrix}$$

$$\mathbf{B} = \begin{bmatrix} \frac{R}{L}(1-d_o) & \frac{1}{L} \\ \frac{R}{L}(1-d_o) & 0 \\ -\frac{1}{C}(1-d_o) & 0 \\ -\frac{1}{C}(1-d_o) & 0 \end{bmatrix}, \quad \mathbf{x} = \begin{bmatrix} i_{L_1} \\ i_{L_2} \\ v_{C_1} \\ v_{C_2} \end{bmatrix} \quad \mathbf{u} = \begin{bmatrix} i_{load} \\ v_{in} \end{bmatrix},$$

$$\mathbf{y} = \begin{bmatrix} i_{L_1} \\ v_{C_1} \end{bmatrix}, \quad \mathbf{C} = \begin{bmatrix} 1 & 0 & 0 & 0 \\ 0 & 0 & 1 & 0 \end{bmatrix}, \quad \mathbf{D} = \begin{bmatrix} 0 \\ 0 \end{bmatrix}$$

The dynamic state variables and inputs can be expressed as the sum of the steady state and perturbations of the variables from the equilibrium point($x = X + \tilde{x}$) as following.

$$\frac{d}{dt}(\mathbf{X} + \tilde{\mathbf{x}}) = \mathbf{A}(\mathbf{X} + \tilde{\mathbf{x}}) + \mathbf{B}(\mathbf{U} + \tilde{\mathbf{u}}) \tag{2}$$

Where $\mathbf{X} = \begin{bmatrix} I_{L_1} \\ I_{L_2} \\ V_{C_1} \\ V_{C_2} \end{bmatrix}$ is steady-state state variables of the qZSI.

$\tilde{\mathbf{x}} = \begin{bmatrix} \tilde{I}_{L_1} \\ \tilde{I}_{L_2} \\ \tilde{v}_{C_1} \\ \tilde{v}_{C_2} \end{bmatrix}$ is perturbations of the state variables from the equilibrium point of the qZSI. $\mathbf{U} = \begin{bmatrix} I_{load} \\ V_{in} \end{bmatrix}$ is steady-state input of the qZSI. $\tilde{\mathbf{u}} = \begin{bmatrix} \tilde{I}_{load} \\ \tilde{v}_{in} \end{bmatrix}$ is perturbations of the input from the equilibrium point of the qZSI. and $d_0 = D_0 + \tilde{d}_0$ is the shoot-through duty cycle of the qZSI.

The dc-side model of the qZSI can be derived using state space averaging, as seen in Eq. (3).

$$\begin{bmatrix} -(r+R) & 0 & (D_0-1) & D_0 \\ 0 & -(r+R) & D_0 & (D_0-1) \\ (1-D_o) & -D_o & 0 & 0 \\ -D_o & (1-D_o) & 0 & 0 \end{bmatrix} \begin{bmatrix} i_{L_1} \\ i_{L_2} \\ v_{C_1} \\ v_{C_2} \end{bmatrix} + \begin{bmatrix} R(1-D_o) & 1 \\ R(1-D_o) & 0 \\ (D_0-1) & 0 \\ (D_0-1) & 0 \end{bmatrix} \begin{bmatrix} i_{load} \\ v_{in} \end{bmatrix} = 0 \tag{3}$$

The solution to Eq. (3) can be given as follows:

$$\begin{aligned} V_{C_1} &= \frac{1-D_0}{1-2D_0}\, V_{in} - V_R \\ V_{C_2} &= \frac{D_0}{1-2D_0}\, V_{in} - V_R \\ I_L = I_{L_1} &= I_{L_2} = \frac{1-D_0}{1-2D_0} I_{load} \end{aligned} \tag{4}$$

$$\text{where} \quad V_R = \frac{(1-D_0)\,(r+2D_0R)}{(1-2D_0)^2} I_{load}$$

The maximum value of the DC voltage at the input terminals of the inverter, denoted as V_{DC}, can be determined using Eq. (4)

$$V_{DC} = V_{C1} + V_{C2} = BV_{in} - 2V_R \tag{5}$$

$$\text{Since B} = \frac{1}{1-2D_0} \text{ is the boost factor of the qZSI.}$$

The currents flowing through the two inductors in the quasi-Z source network are identical at a stable condition. In addition, if we ignore the resistances that occur in capacitors and the unused resistances that occur in inductors, that is $V_R = 0$. In the buck conversion mode of the qZSI, when the inverter is fully active (as shown in Fig. 2, the diode will conduct, and the voltage across capacitor C_1 is going to be equal to the input voltage, while the voltage across capacitor C_2 will be zero as shown in Fig. 3. To increase V_{DC}, one may keep the six active states as they are and exchange some or all of the two conventional zero states with shoot-through states. The boost factor, denoted as B, is directly proportional to the shoot-through duty ratio, as indicated in Eq. (5). The boost conversion mode of the qZSI is the term used to describe this.

The small-signal state equations can be derived by perturbing from the equilibrium point, as stated in Eq. (6). It is observed from the small signal model that the response of the inductance currents is different. Still, in the steady state, the response is similar (see Eq.(6)). These two cases in Z Source Inverter (ZSI) are the same, so it increases the reliability of

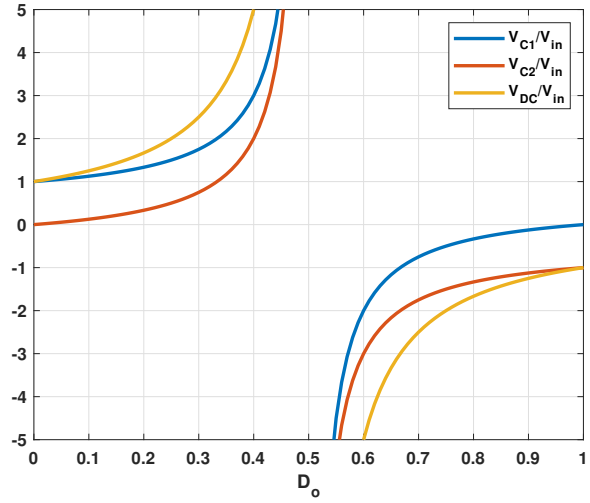

Fig. 3. Plots between $\frac{V_{C1}}{V_{in}}$, $\frac{V_{C2}}{V_{in}}$, and $\frac{V_{DC}}{V_{in}}$ with shoot through ratio.

qZSI and protects the circuit from damage [21].

$$\begin{aligned} &d/dt \begin{bmatrix} \tilde{i}_{L_1} \\ \tilde{i}_{L_2} \\ \tilde{v}_{C_1} \\ \tilde{v}_{C_2} \end{bmatrix} \\ &= \begin{bmatrix} -((r+R))/L & 0 & -\frac{1}{L}(1-D_0) & \frac{1}{L}D_0 \\ 0 & -\frac{(r+R)}{L} & \frac{1}{L}D_0 & -\frac{1}{L}(1-D_0) \\ \frac{1}{C}(1-D_0) & -\frac{1}{C}D_0 & 0 & 0 \\ -\frac{1}{C}D_0 & \frac{1}{C}(1-D_0) & 0 & 0 \end{bmatrix} \\ &\begin{bmatrix} \tilde{I}_{L_1} \\ \tilde{L}_{L_2} \\ \tilde{v}_{C_1} \\ \tilde{v}_{C_2} \end{bmatrix} + \begin{bmatrix} \frac{R}{L}(1-d_0) & \frac{1}{L} \\ \frac{R}{L}(1-d_0) & 0 \\ -\frac{1}{L}(1-d_0) & 0 \\ -\frac{1}{L}(1-d_0) & 0 \end{bmatrix} \begin{bmatrix} \tilde{i}_{Load} \\ \widetilde{V}_{in} \end{bmatrix} \\ &+ \begin{bmatrix} \frac{(V_{C_1}+V_{C_2}-I_{Load}R)}{L} \\ \frac{(V_{C_1}+V_{C_2}-I_{Load}R)}{L} \\ \frac{(-2I_L+I_{Load})}{C} \\ \frac{(-2I_L+I_{Load})}{C} \end{bmatrix} d_o \end{aligned} \tag{6}$$

2) *Small Signal Transfer Functions*

Then achieve the needed power and enhance the capabilities, a closed-loop control system for the shoot-through duty cycle is created based on the previously derived small-signal voltage and current model, neglecting the second-order elements. From a control viewpoint, the input voltage and load current disturbances can be seen as external disturbances that can be immediately compensated for by controllers, and hence,

they are discarded. By the small-signal model, the transfer functions from $\tilde{d}_0$ to the voltage across capacitors $\tilde{v}_{C_1}$ and $\tilde{v}_{C_2}$ are the same and expressed as $\tilde{v}_C$, indicated as Eq. (7).

$$G_1 = \left.\frac{\tilde{v}_C(s)}{\tilde{d}_0(s)}\right|_{\substack{\tilde{i}_{load}=0 \\ \tilde{v}_{in}=0}} = \frac{(V_{C_1}+V_{C_2}-RI_{load})(1-2D_0)+(I_{load}-2I_L)(Ls+r+R)}{LCs^2+C(r+R)s+(1-2D_0)^2} \tag{7}$$

To accurately depict the changing properties of the quasi-Z-source network, we analyse several root loci of the transfer function G(s) by systematically varying the parameters L, C, and D_0. The system parameters are listed as follows: L = 500 µH, C = 400 µF, R = 0.03 Ω, r= 0.47 Ω, D_0= 0.25, I_{load} = 9.9 A, and V_{in}= 130 V. Fig. 2 demonstrates the movement of poles and zeros towards the imaginary axis as the inductance L is changed from 200 μH to 500 μH.
At an inductance value of 100 μH, the poles become equal, resulting in the system being in critical damping, and increasing the inductance to 100 μH results in the emergence of imaginary component the poles, leading to under-damping. Thus, when examining the step response of the function see in Fig. 4, the output waveform exhibits inconsistent overshoot at 100 μH. As the inductance increases, both the overshoot and settling time also increase. The moving of zeros increases the non-minimum-phase undershoots, while the shifting of poles enhances the system settling time and response.

By increasing the capacitance C from 100 μF to 500 μF, Fig.5 demonstrates the vertical movement of the poles towards real axis while the zeros remain unchanged. Increasing system damping has been seen to decrease the amplitude of overshoot and undershoot, but it will also increase the rising time. To ensure appropriate performance and stability, it is crucial to analyze the movements of zero and pole for sources with more comprehensive operating ranges. The same conclusion can be obtained when changing the value of cycle period shown in Fig. 6.
The selection of L and C values in a quasi-Z-source network can be based on a compromise between the damping response and settling time of the transfer function G(s), as determined from the pole-zero maps and step signal test of the derived transfer function.

3) Simple Boost Modulation

The simple boost approach [20] utilises two straight lines that have a value equal to or greater than the peak value of the three phase references as shown in Fig. 7. These lines are utilised to insert the shoot-through duty ratio. By following

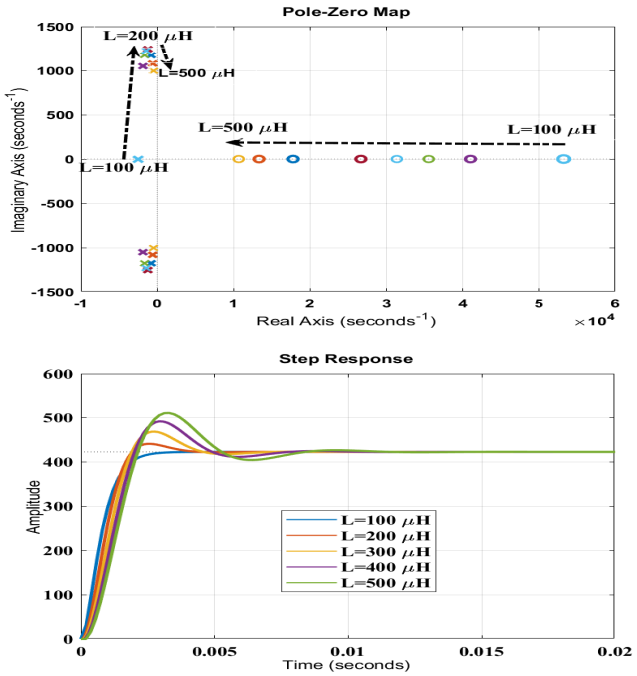

Fig. 4. Changing of inductance with constant outer parameters in qZSI (a) pole-zero mapping ,(b) step response.

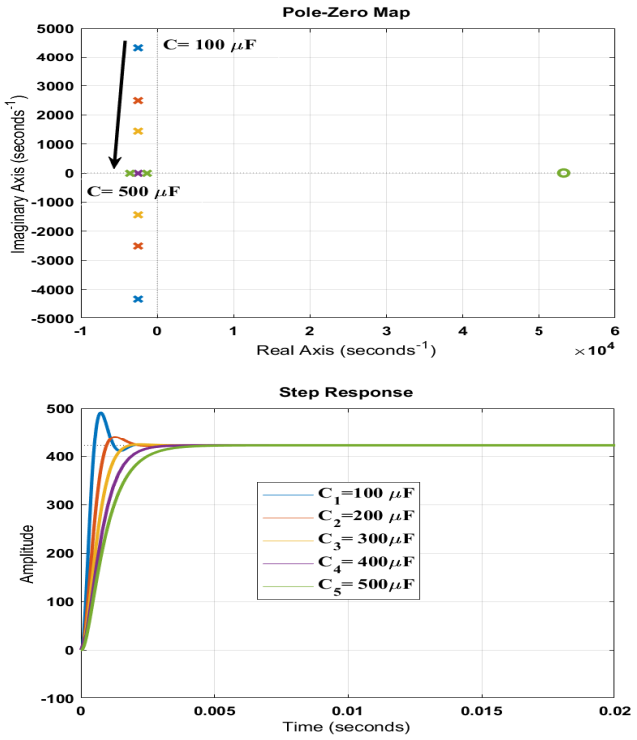

Fig. 5. Changing of capacitance with constant outer parameters in qZSI(a) pole-zero mapping ,(b) step response.

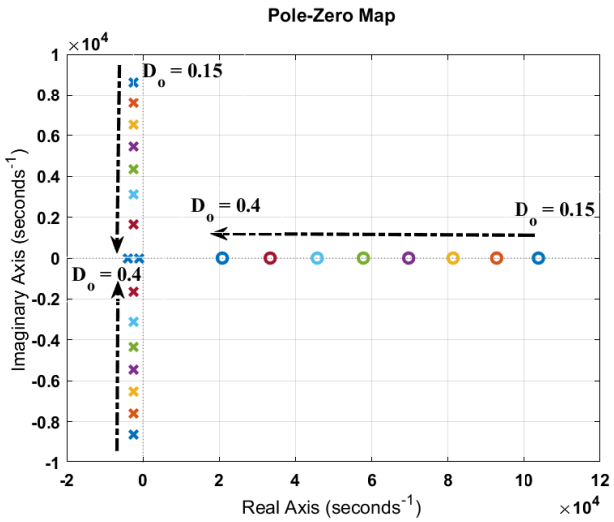

Fig. 6. Changing of duty cycle with constant outer parameters in qZSI.

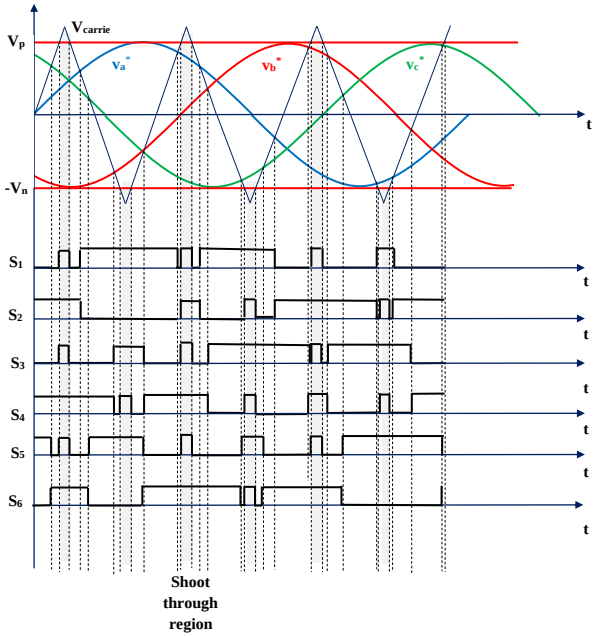

Fig. 7. Simple boost modulation of qZSI circuit.

this approach, the duration of shoot-through time remains consistent for each switching cycle, ensuring a steady boost factor. The shoot-through duty ratio drops as the modulation index M increases in this manner. Therefore, the highest possible shoot-through duty ratio is restricted to (1 - M). When the value of M grows to its maximum, the shoot-through duty ratio reaches zero, causing the inverter to operate in the same way as the typical VSI. The direct current (DC) inductor current and capacitor voltage do not exhibit any fluctuations that are linked to the output frequency.

4) Three-phase grid-tied VSI

Fig. 1 clearly shows that the dc-link voltage of the VSI corresponds to the output voltage of the qZS network. The Voltage Source Inverter (VSI) is linked to the electrical grid through a Low Pass Filter (LCL). By utilising Kirchhoff's voltage and current rules to analyse the circuit depicted on the right of the qZS network, one can derive the subsequent set of differential equations.

$$L_1\frac{di_1}{dt}+r_1i_1=V_{inv}-V_C \tag{8}$$

$$L_o\frac{di_o}{dt}+r_oi_o=V_C-V_g \tag{9}$$

$$C\frac{dV_C}{dt}=i_i-i_o \tag{10}$$

Where the matrices are given by $\mathbf{i_i}=\begin{bmatrix}i_{ia} & i_{ib} & i_{ic}\end{bmatrix}^T$, $\mathbf{V_{inv}}=\begin{bmatrix}v_{an} & v_{bn} & v_{cn}\end{bmatrix}^T$, $\mathbf{V_C}=\begin{bmatrix}v_{ca} & v_{cb} & v_{cc}\end{bmatrix}^T$, $\mathbf{i_o}=\begin{bmatrix}i_{oa} & i_{ob} & i_{oc}\end{bmatrix}^T$, $\mathbf{V_g}=\begin{bmatrix}v_{ga} & v_{gb} & v_{gc}\end{bmatrix}^T$, $\mathbf{L_i}=\begin{bmatrix}L_{ia} & L_{ib} & L_{ic}\end{bmatrix}$, $\mathbf{L_o}=\begin{bmatrix}L_{oa} & L_{ob} & L_{oc}\end{bmatrix}$, and $C=\begin{bmatrix}C_a & C_b & C_c\end{bmatrix}$ respectively. The three-phase grid voltage are given by $v_{ga}=V_g\cos(\omega t)$, $v_{gb}=V_g\cos\left(\omega t-\frac{2\pi}{3}\right)$, and $v_{gc}=V_g\cos\left(\omega t+\frac{2\pi}{3}\right)$ since the current injected into the grid is required to be sinusoidal and in phase with the grid voltage so the reference grid current should be selected as following $i_{oa}{}^*=I_o^*\cos(\omega t)$, $i_{ob}{}^*=I_o^*\cos\left(\omega t-\frac{2\pi}{3}\right)$, and $i_{oc}{}^*=I_o^*\cos\left(\omega t+\frac{2\pi}{3}\right)$.
The pole voltages can be obtained as $V_{IN}=\frac{1}{2}(1+s_k)V_{dc}$ as k=a,b,c and s_k is switching function given by the following equation

$$s_k=\begin{cases}+1 \text{ if } s_i \text{ is closed}\\ -1 \text{ if } \overline{s_i} \text{ is closed}\end{cases}$$

Since $V_{inv}=V_{iN}-V_{nN}$
So, The phase to neutral voltage expressions in terms of input voltage and switching function

$$V_{inv}=\frac{1}{6}V_{dc}\begin{bmatrix}2 & -1 & -1\\ -1 & 2 & -1\\ -1 & -1 & 2\end{bmatrix}\begin{bmatrix}s_a\\ s_b\\ s_c\end{bmatrix} \tag{11}$$

It can be transformed the three-phase quantity to the synchronous reference dq frame oriented by d-axis and neglected zero sequence component so the all AC quantities become DC hence this purpose using Park transformation to obtain different variables of this circuit. Applying this transformation can

be written as:

$$\begin{bmatrix} i_{xd} \\ i_{xq} \end{bmatrix} = \frac{2}{3}\mathbf{T}\begin{bmatrix} i_{xa} \\ i_{xb} \\ i_{xc} \end{bmatrix} \quad \text{where x reperesent i or o}$$

$$\begin{bmatrix} v_{yd} \\ v_{yq} \end{bmatrix} = \frac{2}{3}\mathbf{T}\begin{bmatrix} v_{ya} \\ v_{yb} \\ v_{yc} \end{bmatrix} \text{ where y reperesent g or c}$$

$$\begin{bmatrix} S_d \\ S_q \end{bmatrix} = \frac{2}{3}\mathbf{T}\begin{bmatrix} S_a \\ S_b \\ S_c \end{bmatrix}, \text{ and}$$

$$\mathbf{T} = \begin{bmatrix} \cos(\omega t) & \cos\left(\omega t - \frac{2\pi}{3}\right) & \cos\left(\omega t + \frac{2\pi}{3}\right) \\ -\sin(\omega t) & -\sin\left(\omega t - \frac{2\pi}{3}\right) & -\sin\left(\omega t + \frac{2\pi}{3}\right) \end{bmatrix}$$

is Park transformation

The conversion of a differential equation from a three-axis system to a two-axis system can be achieved using the following equation.

$$\frac{2}{3}\mathbf{T}\mathbf{L_x}\frac{d}{dt}\begin{bmatrix} i_{xa} \\ i_{xb} \\ i_{xc} \end{bmatrix} = \mathbf{L_x}\frac{d}{dt}\begin{bmatrix} i_{xd} \\ i_{xq} \end{bmatrix} - \omega\mathbf{L_x}\begin{bmatrix} i_{xq} \\ -i_{xd} \end{bmatrix} \quad (12)$$

Multiplying both side of Eq. (11) by Park transformation and making some algebraic manipulation one can obtain the following expression

$$\frac{2}{3}\mathbf{T}\mathbf{V}_{inv} = \frac{1}{2}V_{dc}\begin{bmatrix} S_d \\ S_q \end{bmatrix} \quad (13)$$

Now, the transformation of Eqs. (8) - (10) is given by

$$L_{id}\frac{d}{dt}(i_{id}) + r_{id}i_{id} = \omega L_{id}i_{iq} + \frac{v_{dc}}{2}s_d - v_{cd} \quad (14)$$

$$L_{iq}\frac{d}{dt}(i_{iq}) + r_{iq}i_{iq} = -\omega L_{iq}i_{id} + \frac{v_{dc}}{2}s_q - v_{cq} \quad (15)$$

$$L_{od}\frac{d}{dt}(i_{od}) + r_{od}i_{od} = \omega L_{od}i_{oq} + v_{cd} - v_{gd} \quad (16)$$

$$L_{oq}\frac{d}{dt}(i_{oq}) + r_{oq}i_{oq} = -\omega L_{oq}i_{od} + v_{cq} - v_{gq} \quad (17)$$

$$C_d\frac{d}{dt}(v_{cd}) = i_{id} - i_{od} + \omega C_d v_{cq} \quad (18)$$

$$C_q\frac{d}{dt}(v_{cq}) = i_{iq} - i_{oq} - \omega C_q v_{cd} \quad (19)$$

Assume that $L_{id} = L_{iq} = L_i$, $L_{od} = L_{oq} = L_o$, $r_{id} = r_{iq} = r_i$, $r_{od} = r_{oq} = r_o$,and $C_{cd} = C_{cq} = C$ in Eqs. (14) - (19). The control input is defined as sum of steady-state and perturbed quantities

$$s_d = S_d + \Delta s_d \quad (20)$$

$$s_q = S_q + \Delta s_q \quad (21)$$

Assuming that the inverter, grid currents, and capacitor voltage track their references in steady-state and all parameters of inverter and grid inductances and capacitance in two-axis are equal, then steady-state switching functions can be expressing Eqs. (14) and (15) as following

$$S_d = \frac{2}{v_{dc}}\left[L_{ie}\frac{d}{dt}(i_{id}^*) + r_{ie}i_{id}^* + v_{cd}^* - \omega L_{ie}i_{iq}^*\right] \quad (22)$$

$$S_q = \frac{2}{v_{dc}}\left[L_{ie}\frac{d}{dt}(i_{iq}^*) + r_{ie}i_{iq}^* + v_{cq}^* + \omega L_{ie}i_{id}^*\right] \quad (23)$$

Where $L_{ie}$and r_{ie} are estimate inductance and resistance respectively and i_{id}^*,i_{iq}^*, v_{cd}^*,and v_{cq}^* are inverter currents and capacitor voltages, then v_{cd}^*,and v_{cq}^* can be written from Eqs. (16) and (17).

$$v_{cd}^* = L_{oe}\frac{d}{dt}(i_{od}^*) + r_{oe}i_{od}^* - \omega L_{oe}i_{oq}^* + v_{gd} \quad (24)$$

$$v_{cq}^* = L_{oe}\frac{d}{dt}(i_{oq}^*) + r_{oe}i_{oq}^* + \omega L_{oe}i_{od}^* + v_{gq} \quad (25)$$

The grid reference current can be converted from a three-phase system into two phases, so this current can be expressed as components dq synchronous reference frame oriented with grid voltage as following $i_{od}^* = I_o^*, i_{oq}^* = 0$ and grid voltage is given by $v_{gd} = V_g$, $v_{gq} = 0$. By substituting the aforementioned relationships into Eqs. (18)-(19) and (22)-(25) to get

$$v_{cd}^* = r_{oe}I_o^* + V_g \quad (26)$$

$$v_{cq}^* = \omega L_{oe}I_o^* \quad (27)$$

$$i_{id}^* = I_o^*\left(1 - \omega^2 C_e L_{oe}\right) \quad (28)$$

$$i_{iq}^* = \omega C_e r_{oe}I_o^* + \omega C_e V_g \quad (29)$$

$$S_d = \frac{2}{V_{dc}}\left[I_o^*\left\{r_{ie}\left(1-\omega^2 C_e L_{oe}\right)+r_{oe}\left(1-\omega^2 C_e L_{ie}\right)\right\}+ V_g\left(1-\omega^2 C_e L_{ie}\right)\right] \tag{30}$$

$$S_q = \frac{2}{V_{dc}}\left[I_o^*\left\{r_{ie}\omega C_e r_{oe}+\omega L_{oe}+\omega L_{ie}\left(1-\omega^2 C_e L_{oe}\right)\right\}+ \omega C_e r_{ie} V_g\right] \tag{31}$$

Equations (30) and (31) represented the switching function in steady-state then to find the perturbation state must use the Lyapunov function. The state variables are clearly defined as $x_1 = i_{id} - {i_{id}}^*$, $x_2 = i_{iq} - {i_{iq}}^*$,$x_3 = i_{od} - {i_{od}}^* = i_{od} - I_o^*$, $x_4 = i_{oq} - {i_{oq}}^* = i_{oq}$, $x_5 = v_{cd} - {v_{cd}}^*$, $x_6 = v_{cq} - {v_{cq}}^*$.

5) Lyapunov-function based control

The dynamics of a system near its equilibrium point are often determined using Lyapunov's direct technique. The equilibrium points of a three-phase grid-tied LCL-filtered qZSI is at ($x_1 = 0$,$x_2 = 0$, $x_3 = 0$, $x_4 = 0$, $x_5 = 0$, $x_6 = 0$). This study aims to establish a control approach that guarantees the overall asymptotic stability of a grid-tied qZSI at its equilibrium point. The state variables converge to the equilibrium point as the total energy of qZSI is continuously dissipated. The qZSI receives its input energy (E_{in}) from the output voltage (V_{dc}) of the qZS network. The energy expended by the components r_i, r_o, R, and transistors of the qZSI system results in a loss of a portion of E_{in}. Nevertheless, the excess energy is conveyed to the grid, denoted as E_g.

Capacitors and inductors can store energy instead of releasing it. Thus, the energy contained within the qZSI is allocated among the components of the LCL filter, namely the inductor (L_i), capacitor (C), and output filter (L_o). This implies that a portion of E_{in} is transferred through the interchange of energy stored in the components (ΔE_{Li}, ΔE_{Lo}, and ΔE_C) in a bidirectional manner until the overall energy dissipation approaches the equilibrium point of the qZSI.

The control strategy ensuring the overall stability of the grid-tied qZSI is determined by employing Lyapunov's direct technique. Lyapunov's direct technique uses a scalar energy-like function known as the Lyapunov function, represented by V (x). According to this approach, a system can be ensured to be asymptotically stable globally if the Lyapunov function fulfils several requirements such as $V(x) = 0$, $V(x) > 0$ at all $x \neq 0$, $V(x) \to 0$ as $|x| \to \infty$,$\dot{V}(x) < 0$ at all $x \neq 0$. Substituting the state variables and Eqs. (20)-(25) into Eqs. (14)-(19) and assume $L_{ie} - L_i = \tilde{L}_i$, $L_{oe} - L_o = \tilde{L}_o$, $r_{ie} - r_i = \tilde{r}_i$, $r_{oe} - r_o = \tilde{r}_o$,and $C_e - C = \tilde{C}$ yield

$$\begin{aligned}
L_i\dot{x}_1 &= -r_i x_1 + \omega L_i x_2 - x_5 + \frac{V_{dc}}{2}\Delta s_d + \tilde{L}_i\frac{d}{dt}\left({i_{id}}^*\right) + \tilde{r}_i {i_{id}}^* - \omega\tilde{L}_i {i_{iq}}^* \\
L_i\dot{x}_2 &= -\omega L_i x_1 - r_i x_2 - x_6 + \frac{V_{dc}}{2}\Delta s_q + \tilde{L}_i\frac{d}{dt}\left({i_{iq}}^*\right) + \tilde{r}_i {i_{iq}}^* + \omega\tilde{L}_i {i_{id}}^* \\
L_o\dot{x}_3 &= -r_o x_3 + \omega L_o x_4 + x_5 + \tilde{L}_o\frac{d}{dt}\left({i_{od}}^*\right) + \tilde{r}_o {i_{od}}^* - \omega\tilde{L}_o i_{oq} \\
L_o\dot{x}_4 &= -\omega L_o x_3 - r_o x_4 + x_6 + \tilde{L}_o\frac{d}{dt}\left({i_{oq}}^*\right) + \tilde{r}_o {i_{oq}}^* + \omega\tilde{L}_o {i_{od}}^* \\
C\dot{x}_5 &= x_1 - x_3 + \omega C x_6 \\
C\dot{x}_6 &= x_2 - x_4 - \omega C x_5
\end{aligned} \tag{32}$$

A Lyapunov function with energy-like properties can be constructed for this system in the following manner.

$$V(x) = \Delta E_{Li} + \Delta E_{Lo} + \Delta E_C = \frac{3}{2}L_i {x_1}^2 + \frac{3}{2}L_i {x_2}^2 + \frac{3}{2}L_o {x_3}^2 + \frac{3}{2}L_o {x_4}^2 + \frac{3}{2}C{x_5}^2 + \frac{3}{2}C{x_6}^2 \tag{33}$$

It is evident that the first three features described above are met in Eq. (33). To fulfil the fourth requirement, the function $\dot{V}(x)$ needs to be determined. Now, differentiating the function $v(x)$ and substituting Eq. (32) yield

$$\dot{V}(x) = \frac{3}{2}x_1 V_{dc}\Delta s_d + \frac{3}{2}x_2 V_{dc}\Delta s_q - 3r_i\left({x_1}^2 + {x_2}^2\right) - 3r_o\left({x_3}^2 + {x_4}^2\right) + 3\tilde{L}_i x_1\left[\frac{d}{dt}\left({i_{id}}^*\right) - \omega {i_{iq}}^*\right] + 3\tilde{L}_i x_2\left[\frac{d}{dt}\left({i_{iq}}^*\right) + \omega {i_{id}}^*\right] + 3\tilde{L}_o x_3\left[\frac{d}{dt}\left({i_{od}}^*\right) - \omega {i_{oq}}^*\right] + 3\tilde{L}_o x_4\left[\frac{d}{dt}\left({i_{oq}}^*\right) + \omega {i_{od}}^*\right] + 3\tilde{r}_i\left[x_1 {i_{id}}^* + x_2 {i_{iq}}^*\right] + 3\tilde{r}_o\left[x_3 {i_{od}}^* + x_4 {i_{oq}}^*\right] \tag{34}$$

Assuming perfect matching between actual and estimation parameters the Eq. (34) can be modified by following

$$\dot{V}(x) = \frac{3}{2}x_1 V_{dc}\Delta s_d + \frac{3}{2}x_2 V_{dc}\Delta s_q - 3r_i\left({x_1}^2 + {x_2}^2\right) - 3r_o\left({x_3}^2 + {x_4}^2\right) \tag{35}$$

It is apparent that the fourth feature, which is the negative definiteness of $V(x)$, would always be ensured if Δs_d and Δs_q were selected as

$$\Delta s_d = K_d V_{dc} x_1 \tag{36}$$

$$\Delta s_q = K_q V_{dc} x_2 \tag{37}$$

Where $K_d < 0$ and $K_q < 0$ are constant.
While Eqs. (36)-(37) can ensure global stability, if there is a parameter mismatch, it is advisable to choose K_d and K_q to be as large as feasible in order to have dominance over the last term in Eq. (34), ensuring that the criterion for $\dot{V}(x)$ to be less than zero is guaranteed. The level of resonance damping is unsatisfactory, in order to address the issue of resonant damping, the authors in [19] suggested incorporating the capacitor voltage feedback into the perturbed switching function in the following manner.

$$\Delta s_d = K_d V_{dc} x_1 - K_{cd} x_5 \tag{38}$$

$$\Delta s_d = K_q V_{dc} x_2 - K_{cq} x_6 \tag{39}$$

Where $K_{cd} > 0$ and $K_{cq} > 0$ are constant. Now, substituting equations (38)-(39) into (35) and assume $K_d = K_q$ and $K_{cd} = K_{cq}$ gives

$$\dot{V}(x) = \frac{3}{2} V_{dc}{}^2 K_d \left(x_1{}^2 + x_2{}^2\right) - \frac{3}{2} V_{dc} K_{cd} \left(x_1 x_5 + x_2 x_6\right) - 3r_i \left(x_1{}^2 + x_2{}^2\right) - 3r_o \left(x_3{}^2 + x_4{}^2\right) < 0 \tag{40}$$

Then, considering that r_1 and r_2 contribute to an extra passive damping effect, the stability of the Lyapunov function would be at its worst if r_1 and r_2 were not there.

$$K_{cd} = K_{cq} > \frac{V_{dc} K_d \left(x_1{}^2 + x_2{}^2\right)}{\left(x_1 x_5 + x_2 x_6\right)} \tag{41}$$

Therefore, the total switching function, which includes both steady-state switching function and perturbed switching function, may be expressed from Eqs. (30)-(31) and Eqs. (38)-(39) yield

$$s_d = \frac{2}{V_{dc}} \left[I_o^* \left\{r_{ie}\left(1 - \omega^2 C_e L_{oe}\right) + r_{oe}\left(1 - \omega^2 C_e L_{ie}\right)\right\} + V_g \left(1 - \omega^2 C_e L_{ie}\right)\right] + K_d V_{dc} x_1 - K_{cd} x_5 \tag{42}$$

$$s_q = \frac{2}{V_{dc}} \left[I_o^* \left\{r_{ie}\omega C_e r_{oe} + \omega L_{oe} + \omega L_{ie}\left(1 - \omega^2 C_e L_{oe}\right)\right\} + \omega C_e r_{ie} V_g\right] + K_q V_{dc} X_2 - K_{cq} X_6 \tag{43}$$

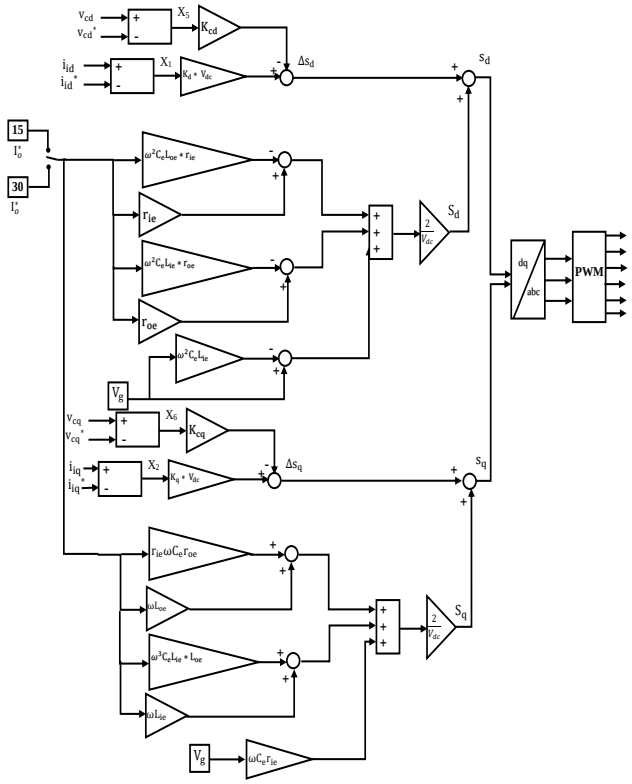

Fig. 8. Control using a Lyapunov-based function.

It is important to mention that the control laws in Eqs. (42)-(43) can accomplish the intended control objectives if the dc link voltage of the qZS network is regulated to the correct level as shown in Fig. 8 (which should be higher than the peak voltage at the inverter output) and the reference function (I_o^*) is accurately produced.

6) Control of qZSI network by shoot-through method

The regulator of shoot-through duty ratio (D_{ST}) is basically in performance wanted operation of the qZSI network, to realize this, the inductance current and capacitance-voltage can be controlled in a circuit. Proportional-Resonant (PR) control can be utilized for this purpose. The fact that a PR controller demonstrates excellent performance in accurately following a reference sinusoidal signal is widely recognized. The transfer function of an ideal (PR) controller is shown in equation below.

$$G_{PR}(s) = K_p + \frac{2 K_r s}{s^2 + \omega^2} \tag{44}$$

The variables K_p and K_r represent the proportional and resonant gains, respectively. The symbol ω represents the resonant frequency. If the frequency of the reference grid current is cho-

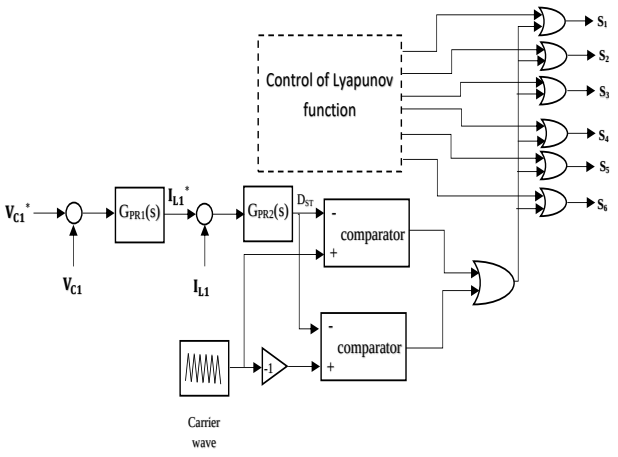

Fig. 9. Control using a Lyapunov function that incorporates shoot through states.

sen as ω, then the PR controller, as specified in equation (44), provides an infinite gain at the resonant frequency ω. This ensures that the grid current precisely follows its reference without any inaccuracy in the steady-state [19]. Nevertheless, it is impractical to implement a PR controller with unrestricted gain. Hence, the subsequent imperfect transfer function is employed in practical applications.

$$G_{PR}(s) = K_p + \frac{2\,K_r\omega_c s}{s^2 + 2\omega_c s + \omega^2} \tag{45}$$

The system utilizes two proportional-resonant (PR) controllers that function based on errors in capacitor voltage and inductor current as described below.

$$G_{PR1}(\,s) = \frac{{I_{L_1}}^*}{{v_{C_1}}^* - V_{C_1}} = K_{p1} + \frac{2\,K_{r1}\omega_c s}{s^2 + 2\omega_c s + \omega^2} \tag{46}$$

and

$$G_{PR2}(\,s) = \frac{D_{ST}}{{I_{L_1}}^* - I_{L_1}} = K_{p2} + \frac{2\,K_{r2}\omega_c s}{s^2 + 2\omega_c s + \omega^2} \tag{47}$$

The cut-off frequency is represented by ω_c, the resonant frequency is represented by ω, and K_{p1}, K_{p2}, K_{r1} and K_{r2} are proportional and resonant gains, respectively. The shoot-through states may be produced by comparing the complement of the duty cycle ($1 - D_{ST}$) with the triangular carrier waveform used for generating PWM signals for the inverter switches as shown in Fig. (9).

III. Results of The Simulation

The simulations of qZSI with LCL-filter-based three-phase grid-connected VSI demonstrate the effectiveness and utility of the suggested control technique. The simulations were done using Matlab/Simulink. A phase locked loop (PLL) is utilized to produce the current reference that is synchronized with the grid voltage and frequency. The switching function of the proposed control method is computed after producing the requisite reference signals $\left({i_{id}}^*, {i_{iq}}^*, {v_{cd}}^* \text{ and } {v_{cq}}^*\right)$ and used Lyapunov function based control. Next, the PWM signals are generated by comparing the calculated switching function with a carrier wave that has a frequency of 12.5 kHz . The controller gains were assigned the following values: $K_d = K_q = -0.004$, $K_{cd} = K_{cq} = 4$, $K_{p1} = 1.5$, $K_{p2} = 3, K_{r1} = 80$, $K_{r2} = 500$, and $\omega_c = 1\text{rad/s}$. The system parameters are shown in Table. I.

TABLE I.
System Parameters

Symbol	Value
DC link voltage, V_{dc}	800 V
Inductance on the side of the inverter, L_i	1.4 mH
Inductance on the grid side, L_o	0.5 mH
Capacitance of the filter, C	50μF
Inverter inductor resistors, r_i	0.1Ω
Grid inductor resistors, r_o	0.05Ω
Switching frequency	12.5 kHz
Amplitude of the grid voltage, V_g	$230 * \sqrt{2}$
Inductances of the gZS network, L_1, L_2	500μH
Capacitances of the gZZ network, C_1, C_2	400μF

Figures (10)-(12) illustrate the dynamic behaviour of the grid voltages and currents when the grid current reference amplitude (I_o^*) is increased from 15 A to 30 A at 0.3 sec . Fig. 10 displays the simulated steady-state responses of the grid voltage and current produced using the Lyapunov-based control method with proportional-resonant (PR) control of qZSI (without capacitor voltage loop). It is assumed that the estimated lower control limit (LCL) parameters are in agreement with the actual parameters. The relationship between the injected grid current and the grid voltage is evident as they are in phase. The oscillations observed in the grid current indicate that the Lyapunov-based control technique, using PR control of qZSI, fails to effectively mitigate the resonance.
Fig. 11 displays the simulated steady-state responses of the grid voltage and current achieved by the suggested control approach with the capacitor voltage loop, assuming that the

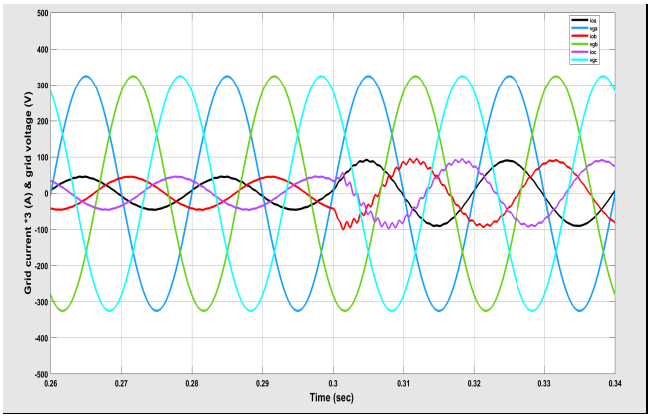

Fig. 10. Simulation of three-phase grid voltage and grid current without capacitor voltage loop.

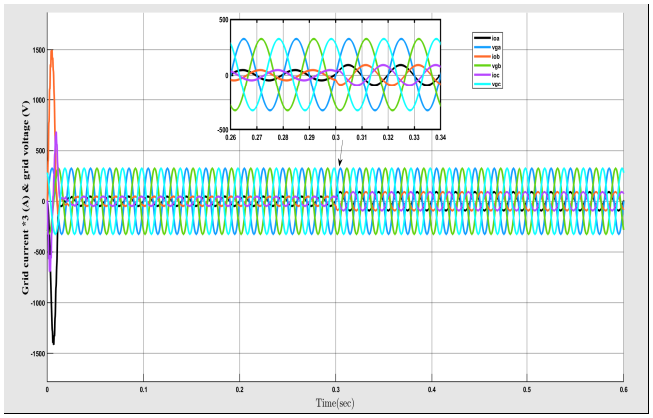

Fig. 11. Simulation of three-phase grid voltage and grid current with capacitor voltage loop.

predicted values are in agreement with the real parameters. By comparing the grid currents shown in Fig. 10 and Fig. 11 , it is evident that the grid current achieved by the suggested control approach does not exhibit oscillations. This indicates a significant improvement in resonance damping. Fig. 12 displays the simulated steady-state responses of the grid voltage and current using the suggested control approach with the capacitor voltage loop. These responses are produced when the estimated parameters deviate from the real parameters by 15% ($L_{ie} = 1.61\text{mH}, L_{oe} = 0.575\text{mH}$, $r_{ie} = 0.115\Omega, r_{oe} = 0.0575\Omega$, and $C_e = 57.5\mu\text{F}$). The control system is most affected by parameter fluctuations when all of the changes occur simultaneously. Regardless of the variations in these parameters, the grid currents exhibit nearly the same amplitude and are in phase with the grid voltages, as shown in Fig. 11. The efficiency of Lyapunov-based control in following the grid current reference is demonstrated, even in the presence of parameter fluctuations.

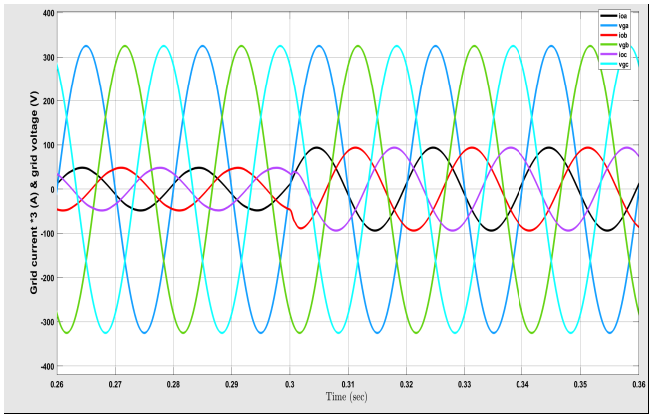

Fig. 12. Simulated response of three phase grid voltage and grid current obtained by the proposed control strategy when there is 15% variation in LCL filter parameters.

Fig. 13 displays the simulated response of $\dot{V}(x)$ in change of reference current, which corresponds to the scenario depicted in Fig. 12. Despite a 15% fluctuation in the parameters of the LCL filter, the value of $\dot{V}(x)$ remains negative, indicating that the suggested control method is globally asymptotically stable.

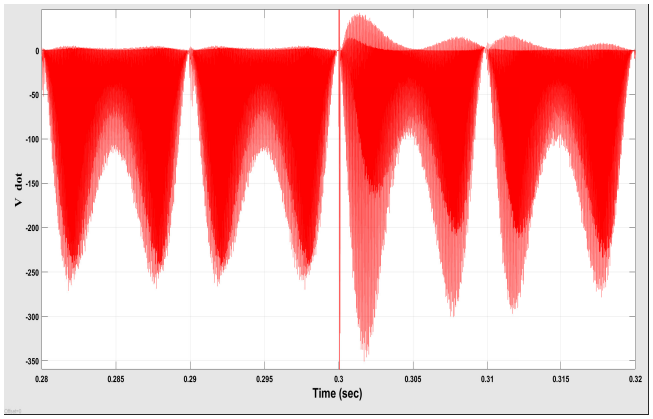

Fig. 13. Response simulating $\dot{V}(x)$ in two cycles.

The spectral analysis of the grid current, with a value of $I_o^* = 30$ A, is depicted in Fig. (14). The total harmonic distortion (THD) of the grid current in phase a, as determined through simulation, was 0.09%, this is smaller than the amount shown in [19]. It is known that the main component of the grid current is approximately 30 A , indicating the absence of any steady-state inaccuracy in the grid current. The other components (3rd, 5th, and 7th) are insignificantly small.

Fig. 15 and Fig. 16 show the d-q axis grid current and d-q capacitor voltage, respectively, in the d-axis synchronous reference frame. These graphs demonstrate the precise tracking of the actual signal to the reference value, with minimal

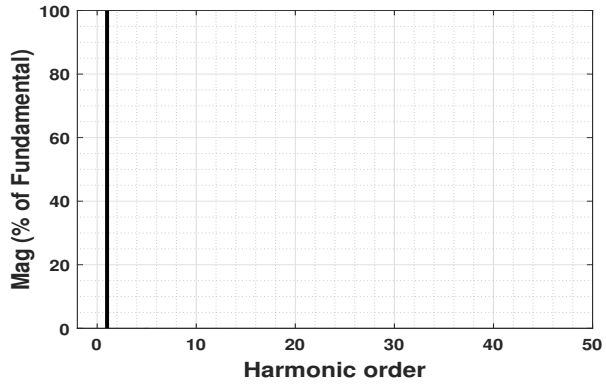

Fig. 14. The spectrum of the grid current phase A.

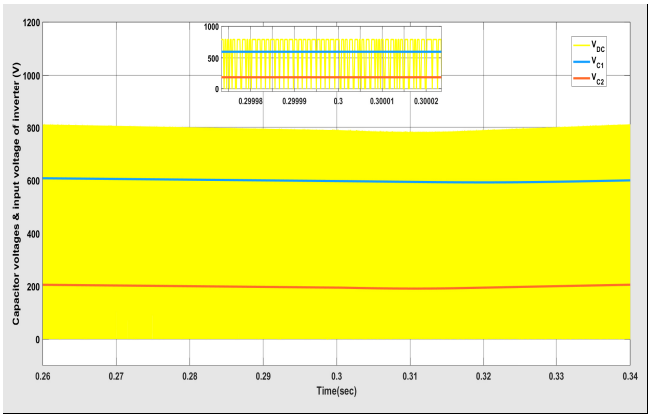

Fig. 17. Responses of capacitors and output voltage of qZS network variables.

overshoot and settling time.

Fig. 17 displays the steady-state responses of the qZS net-

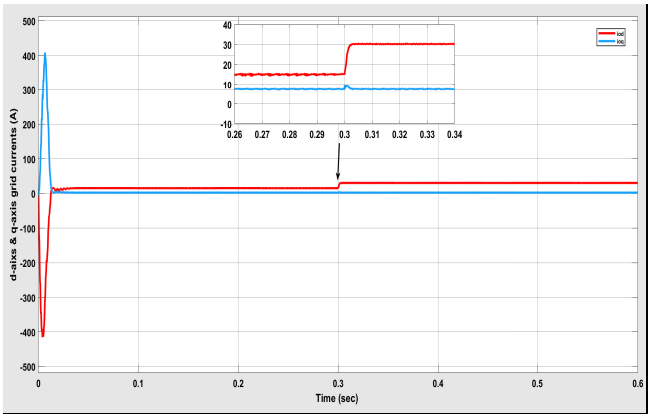

Fig. 15. d-q axis grid current.

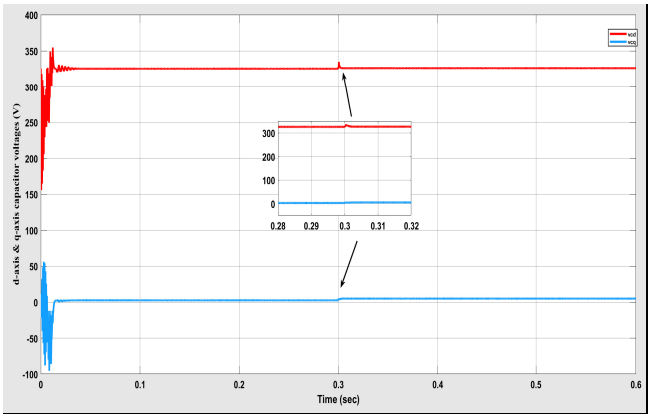

Fig. 16. d-q axis capacitor voltage.

work variables for $V_{C1} = 600$ V and $V_{C2} = 200$ V. Once again, it is evident that the successful control of V_{C1} and V_{C2} has been accomplished and the total of the voltages across two capacitors is equal to the input voltage applied to the inverter.

Fig. 18 illustrates the relationship between grid current total harmonic distortion (THD) and K_{cd}, as determined through scientific means, for various Io values. The total harmonic distortion (THD) values observed for a current of 10A are slightly higher than those reported for a current of 20A, given the identical K_{cd} values. It is evident that Fig. 17 can be partitioned into two distinct sections. Within the initial region, the total harmonic distortion (THD) of the grid current reduces when the value ofK_{cd} is raised from 2 to 4. As the value of K_{cd} is raised from 4 to 6 in the second region, the total harmonic distortion (THD) of the grid current begins to rise. The evidence indicates that increasing K_{cd} can have both beneficial and detrimental impacts on the damping of the capacitor voltage loop.

The suggested control strategy has been compared to existing linear and nonlinear control methods, including the active damping method proposed in [4], the SMC-based control method proposed in [8], the composite nonlinear feedback control method proposed in [10], and the feedback-based PR current control method proposed in [16]. Tables II presents a summary of the comparison between four control methods and the suggested control approach. The proposed control approach, which combines both linear and nonlinear control strategies, presents numerous advantages in comparison to using linear and nonlinear control strategies alone.

IV. Conclusion

The suggested method utilizes a Lyapunov function to operate a three-phase grid-tied qZSI (quasi-Z-source inverter) with an LCL (inductor-capacitor-inductor) filter. While the utilization of LCL filter offers notable benefits, it also presents certain downsides, including the potential for instability and

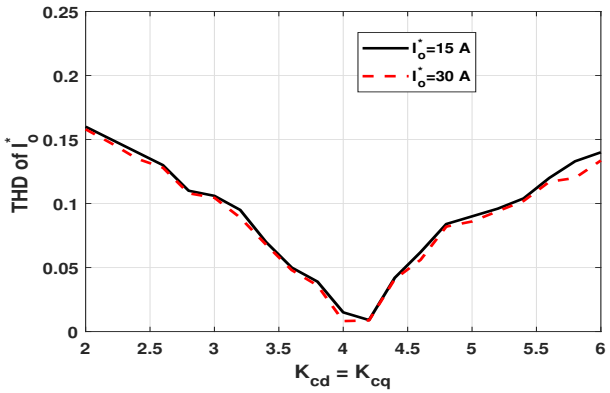

Fig. 18. The relationship between the total harmonic distortion (THD) of grid current and the coefficient of capacitor feedback loop (K_{cd}) is examined for different values of I_o^*.

TABLE II.
COMPARISONS BETWEEN FOUR CONTROL STRATEGIES AND THE PROPOSED CONTROL STRATEGY.

Type of comparison	[4]	[8]	[10]	[16]	Suggested control approach
Robustness	unreported	Excellent	unreported	unreported	Excellent
Asymptotical Global stability	unreported	non-existent	unreported	non-existent	Guaranteed
Damping resistor	Not needed	Not needed	Not needed	needed	Not needed
Responsive behavior	Rapid	Very fast	Very fast	Rapid	Very fast
Harmonic rejection	Good	non-existent	non-existent	non-existent	Very good

heightened control intricacy. The suggested control mechanism ensures the overall stability of the closed-loop system. Furthermore, it incorporates two loops that are dependent on the current loop of the ac-side inverter and the voltage loop of the capacitor. These loops contribute to achieving a desirable level of damping performance. The control of the direct current (dc) side is achieved by the utilization of a straightforward boost control mechanism. The closed-loop system is regulated by integrating the shoot through states with the PWM signal acquired by the Lyapunov function-based control approach. Theoretical considerations have been confirmed through computer simulations conducted during steady-state operation and a sudden alteration in the amplitude of the reference grid current. The findings provided indicate that the control strategy offered is highly effective in attaining the required control objectives for grid-tied qSZI.

CONFLICT OF INTEREST

The authors have declared no conflict of interest.

REFERENCES

[1] A. K. Abdulabbas, S. M. Salih, and M. A. Alawan, "The analysis of sub-synchronous resonance in a wind farm for a doubly-fed induction generator using modern analytical method," *Iraqi Journal for Electrical And Electronic Engineering*, vol. 20, no. 1, 2024.

[2] F. Marignetti, R. L. Di Stefano, G. Rubino, and R. Giacomobono, "Current source inverter (csi) power converters in photovoltaic systems: A comprehensive review of performance, control, and integration," *Energies*, vol. 16, no. 21, p. 7319, 2023.

[3] S. Huang, F. Tang, Z. Xin, Q. Xiao, and P. C. Loh, "Grid-current control of a differential boost inverter with hidden lcl filters," *IEEE Transactions on Power Electronics*, vol. 34, no. 1, pp. 889–903, 2018.

[4] J. Xu, S. Xie, and T. Tang, "Active damping-based control for grid-connected *lcl*-filtered inverter with injected grid current feedback only," *IEEE Transactions on Industrial Electronics*, vol. 61, no. 9, pp. 4746–4758, 2013.

[5] M. Ozturk, F. Zungor, B. Emre, and B. Oz, "Quasi resonant inverter load recognition method," *IEEE Access*, vol. 10, pp. 89376–89386, 2022.

[6] M. Turzynski and P. J. Chrzan, "Reducing common-mode voltage and bearing currents in quasi-resonant dc-link inverter," *IEEE Transactions on Power Electronics*, vol. 35, no. 9, pp. 9553–9562, 2020.

[7] L. Liu, J. Xu, J. Ye, and A. Shen, "Passivity enhancement and grid-current distortion mitigation for inverter-side current controlled lcl-type grid-connected inverters," *IEEE Access*, 2024.

[8] M. A. Estrada, J. A. Moreno, and L. Fridman, "Sliding mode controllers design based on control lyapunov functions for uncertain lti systems," *IFAC-PapersOnLine*, vol. 56, no. 2, pp. 1615–1620, 2023.

[9] S. Prakash, J. K. Singh, and R. K. Behera, "Lyapunov function based control strategy for single-phase grid-connected pv system with lcl-filter," in *2020 IEEE International Conference on Power Electronics, Drives and Energy Systems (PEDES)*, pp. 1–6, IEEE, 2020.

[10] S. Eren, M. Pahlevaninezhad, A. Bakhshai, and P. K. Jain, "Composite nonlinear feedback control and stability analysis of a grid-connected voltage source inverter with lcl filter," *IEEE Transactions on Industrial Electronics*, vol. 60, no. 11, pp. 5059–5074, 2012.

[11] S. Bayhan, M. Trabelsi, H. Abu-Rub, and M. Malinowski, "Finite-control-set model-predictive control for a quasi-z-source four-leg inverter under unbalanced load condition," *IEEE Transactions on Industrial Electronics*, vol. 64, no. 4, pp. 2560–2569, 2016.

[12] S. P. Sonkar, V. Lal, and R. Singh, "Three phase quasi z source inverters with multiple ac outputs," in *2019 IEEE Energy Conversion Congress and Exposition (ECCE)*, pp. 589–595, IEEE, 2019.

[13] G. S. Krishna, M. S. Ballal, S. R. Verma, G. Sharma, H. A. Kale, and K. Naipunya, "Integration of res using multiport dc-dc converter and load management," in *2022 IEEE International Conference on Power Electronics, Drives and Energy Systems (PEDES)*, pp. 1–6, IEEE, 2022.

[14] M. Hosseinpour *et al.*, "Resonance damping of lcl filters using capacitor-current proportional-integral positive feedback method for grid-integrated fuel cell system," *Emirates Journal for Engineering Research*, vol. 28, no. 3, p. 5, 2023.

[15] Y. Liu, B. Ge, H. Abu-Rub, and F. Z. Peng, "Overview of space vector modulations for three-phase z-source/quasi-z-source inverters," *IEEE Transactions on Power Electronics*, vol. 29, no. 4, pp. 2098–2108, 2013.

[16] Y. Li, J. Zhang, Z. Hao, and P. Tian, "Improved pr control strategy for an lcl three-phase grid-connected inverter based on active damping," *Applied Sciences*, vol. 11, no. 7, p. 3170, 2021.

[17] S. Bayhan and H. Komurcugil, "Lyapunov-function-based controller for single-phase npc quasi-z-source inverter with 2 ω frequency ripple suppression," *Energies*, vol. 14, no. 1, p. 140, 2020.

[18] M. Hosseinpour and N. Rasekh, "A single-phase grid-tied pv based trans-z-source inverter utilizing lcl filter and grid side current active damping," *Journal of Energy Management and Technology*, vol. 3, no. 3, pp. 67–77, 2019.

[19] I. Sefa, S. Ozdemir, H. Komurcugil, and N. Altin, "An enhanced lyapunov-function based control scheme for three-phase grid-tied vsi with lcl filter," *IEEE Transactions on Sustainable Energy*, vol. 10, no. 2, pp. 504–513, 2018.

[20] H. Komurcugil, S. Bayhan, and H. Abu-Rub, "Lyapunov-function based control approach with cascaded pr controllers for single-phase grid-tied lcl-filtered quasi-z-source inverters," in *2017 11th IEEE International Conference on Compatibility, Power Electronics and Power Engineering (CPE-POWERENG)*, pp. 510–515, IEEE, 2017.

[21] H. Komurcugil, S. Ozdemir, N. Altin, and I. Sefa, "A modified lyapunov-function based control strategy for three-phase grid-connected vsi with lcl filter," in *IECON 2016-42nd Annual Conference of the IEEE Industrial Electronics Society*, pp. 2218–2223, IEEE, 2016.